

# Compact Binary Formation in Open Star Clusters II: Difficulty of Gaia NS formation in low-mass star clusters

Ataru Tanikawa<sup>1</sup>\*, Long Wang<sup>2,3</sup>, Michiko S. Fujii<sup>1</sup>

<sup>1</sup>Center for Information Science, Fukui Prefectural University, 4-1-1 Matsuoka Kenjojima, Eiheiji-cho, Fukui 910-1195, Japan

<sup>2</sup>School of Physics and Astronomy, Sun Yat-sen University, Daxue Road, Zhuhai, 519082, China

<sup>3</sup>CSST Science Center for the Guangdong-Hong Kong-Macau Greater Bay Area, Zhuhai, 519082, China

<sup>4</sup>Department of Astronomy, Graduate School of Science, The University of Tokyo, 7-3-1 Hongo, Bunkyo-ku, Tokyo 113-0033, Japan

Accepted XXX. Received YYY; in original form ZZZ

## ABSTRACT

Gaia mission offers opportunities to search for compact binaries not involved in binary interactions (hereafter inert compact binaries), and results in the discoveries of binaries containing one black hole (BH) or one neutron star (NS), called “Gaia BHs” and “Gaia NSs”, respectively. We have assessed if Gaia BHs and NSs can be formed in open clusters through dynamical interactions. In order to obtain a large number of inert compact binaries similar to Gaia BHs and NSs, we have performed gravitational  $N$ -body simulations for a large number of open clusters whose total mass is  $1.2 \times 10^8 M_\odot$ . These clusters have various masses, metallicities, densities, and binary fractions. We have found that open clusters form Gaia BHs ( $10^{-6}$ – $10^{-5} M_\odot^{-1}$ ) much more efficiently than Gaia NSs ( $\lesssim 10^{-7} M_\odot^{-1}$ ) for any cluster parameters. This is quite inconsistent with observational results, because the reported numbers of Gaia BHs and NSs are 2 and  $\sim 20$ , respectively. Additionally, we have switched off NS natal kicks for  $10^4$  open clusters each weighing  $10^3 M_\odot$  in order to retain a large number of NSs in open clusters. Then, open clusters form inert NS binaries originating from primordial binaries rather than formed through dynamical interactions. This means that Gaia NSs are formed dominantly on isolated fields, not in open clusters, if there is no NS natal kick. We have concluded that Gaia BHs can be dominantly formed in open clusters, however Gaia NSs cannot.

**Key words:** stars: black holes – galaxies: star clusters: general – Astrometry and celestial mechanics – (stars:) binaries (including multiple): close

## 1 INTRODUCTION

Black holes (BHs) and neutron stars (NSs) are compact objects left behind after the deaths of massive stars. They are clues to physical processes involved in massive star evolution, and experimental sites of strong gravitational fields. Thus, they have been explored vigorously. Because of their darkness, only active BHs and NSs have been discovered until quite recently. Active compact objects can be X-ray binaries (see Casares et al. 2017, for review), gravitational wave sources (Abbott et al. 2019, 2021, 2023), and pulsars (see Philippov & Kramer 2022, for review).

Very recently, inactive compact objects have started to be discovered. Mainly, they are binary members, because they are found through binary motions. They are called “non-interacting”, “detached”, “dormant”, or “inert” compact binaries. Hereafter, we unify the notation with inert compact binaries throughout this paper. Such inert compact binaries have been discovered by spectroscopic observations (Giesers et al. 2018; Shenar et al. 2022), and by astrometric observations (El-Badry et al. 2023b,c; Tanikawa et al. 2023; Chakrabarti et al. 2023) with the help of Gaia DR3 (Gaia Collabora-

tion et al. 2023a,b; see review by El-Badry 2024). Gaia DR3 seems to contain more inert compact binaries according to several candidate lists (Andrews et al. 2022; Shahaf et al. 2023b,a; Jayasinghe et al. 2023; Rowan et al. 2024). Although other inert compact binaries have been reported (Liu et al. 2019; Thompson et al. 2019; Rivinius et al. 2020; Jayasinghe et al. 2021, 2022; Lennon et al. 2022; Saracino et al. 2022), their discoveries have been called into question (Abdul-Masih et al. 2020; Bodensteiner et al. 2020; El-Badry & Quataert 2020, 2021; van den Heuvel & Tauris 2020; El-Badry & Burdge 2022; El-Badry et al. 2022a,b). In addition to inert compact binaries, several single BHs/NSs have been detected by microlensing observations (Lam et al. 2022; Sahu et al. 2022; Howil et al. 2024).

Gaia BH1 and BH2 (hereafter Gaia BHs), which are inert BH binaries discovered from Gaia DR3, and named by El-Badry et al. (2023b,c), have two impacts. First, Gaia BHs have the longest orbital periods among BH binaries discovered so far. In particular, Gaia BH2 breaks the record of BH binary periods by 10 times. These discoveries give the impression that Gaia’s astrometric observations open up a new parameter space of BH binaries. Second, Gaia BHs are hard to form through isolated binary evolution. If Gaia BHs are formed through isolated binary evolution, common envelope ejection should be 10 times less efficient than expected (Chawla et al. 2022; El-

\* E-mail: atrtnkw@gmail.com

Badry et al. 2023b; Shikauchi et al. 2023; but see Kotko et al. 2024). However, a recent study has not supported such inefficient common envelope ejection for stars massive enough to form BHs (Hirai & Mandel 2022). Triple stars (El-Badry et al. 2023b,c; Generozov & Perets 2023) and open clusters (Di Carlo et al. 2023; Rastello et al. 2023; Tanikawa et al. 2024) have been suggested as formation sites of Gaia BHs. Because Gaia BHs are the Galactic disk components, it is difficult to suppose that they are formed in globular clusters and galactic centers.

El-Badry et al. (2024) have discovered Gaia NS1 which is most likely to be the first inert NS binary from Gaia DR3 (Gaia Collaboration et al. 2023b). The NS candidate mass ( $\sim 1.9M_{\odot}$ ) is higher than other inert NS binary candidates which could be a massive white dwarfs (WDs) as described in the literature (Geier et al. 2023; Zheng et al. 2023). Gaia NS1 is hard to form through isolated binary evolution without inefficient common envelope ejection, similarly to Gaia BHs. El-Badry et al. (2024) have also mentioned that they have found about 20 more inert NS binaries, called ‘‘Gaia NSs’’ hereafter. This should imply that Gaia NSs are formed more efficiently than Gaia BHs for the following two reasons. First, the number of Gaia NSs discovered is larger than that of Gaia BHs discovered. Second, Gaia NSs is harder to detect than Gaia BHs, because NSs indicate smaller astrometric signals than BHs; NSs swing around their companions less strongly than BHs due to their smaller masses. Another importance of Gaia NS1 is its eccentricity. The eccentricity is  $\sim 0.1$  (El-Badry et al. 2024), while Gaia BH1 and BH2 have  $\sim 0.5$  (El-Badry et al. 2023b,c). The eccentricity of Gaia NS1 may be too small to be formed through dynamical interactions.

In this paper, we test if open clusters can form Gaia NSs more efficiently than Gaia BHs by means of gravitational  $N$ -body simulations. We have found that the formation rate of Gaia NSs is much smaller than that of Gaia BHs if we adopt the conventional single and binary star models. Open clusters cannot retain enough NSs to form Gaia NSs because of their large natal kicks. In order to retain a sufficiently large number of Gaia NSs in open clusters, we switch off natal kicks of NSs, although this assumption is unrealistic. Nevertheless, the formation rate of Gaia NSs is still comparable to that of Gaia BHs, in contrast to the observational implication.

The structure of this paper is as follows. We describe our simulation method in section 2. We show our results in section 3. We discuss if Gaia NSs can be formed in open clusters in section 4. We summarize this paper in section 5.

## 2 METHOD

We use an  $N$ -body code PETAR (Wang et al. 2020b), which is based on the particle-tree and particle-particle algorithm (Oshino et al. 2011; Iwasawa et al. 2017), and highly parallelized by Framework for Developing Particle Simulator with Message Passing Interface, OpenMP, and Single Instruction Multiple Data (FDPS; Iwasawa et al. 2016, 2020). The slow-down algorithmic regularization method (SDAR; Wang et al. 2020a) treats binary orbits and close encounters in order to keep high accuracy efficiently. The Galactic potential is modeled by GALPY (Bovy 2015). Single and binary star evolutions are implemented with the BSE code (Hurley et al. 2000, 2002; Banerjee et al. 2020). Common envelope evolution is the most important process to form compact binaries. The BSE code deals with common envelope evolution, adopting the  $\alpha$  formalism (Webbink 1984). We adopt  $\alpha_{CE} = 1$  and  $\lambda_{CE}$  of Claeys et al. (2014). The choice of  $\alpha_{CE}$  prevents inert compact binaries from being formed from primordial binaries.

NS population retained in open clusters largely depends on NS natal kicks. Here, we remark NS natal kicks in our model. NSs receive kick velocities at their births because of asymmetric supernova explosions. The kick velocities are quite different between NSs born from electron capture (EC) and core collapse (CC) supernovae (SNe). In our model, a star causes a CCSN when its carbon-oxygen (CO) core exceeds both of the Chandrasekhar mass limit ( $1.44M_{\odot}$  here) and  $0.773M_{c,he} - 0.35M_{\odot}$ , where  $M_{c,he}$  is the He core mass of the star. NSs left behind CCSNe have kick velocity distribution given by a single Maxwellian with  $\sigma_{k,ccsn} = 265 \text{ km s}^{-1}$  (Hobbs et al. 2005). If the NSs acquires on fallback mass, the kick velocities are reduced by  $1 - f_{\text{fallback}}$ , where  $f_{\text{fallback}}$  is the fraction of the fallback mass (Fryer et al. 2012). This prescription is also applied to BH natal kicks. ECSNe (Miyaji et al. 1980; Nomoto 1984, 1987; van den Heuvel 2007) are thought to raise much smaller kick velocities than CCSNe because of slightly asymmetric explosion (Jones et al. 2013; Gessner & Janka 2018). In our model, a star generates an ECSN when it does not cause a CCSN, and its CO core mass is  $\geq 1.6M_{\odot}$ . Their natal kick velocities are expressed by a single Maxwellian with  $3 \text{ km s}^{-1}$  (Podsiadlowski et al. 2004; Gessner & Janka 2018). About 1 % of NSs are formed from ECSNe under the initial mass function we adopt.

NSs with small natal kicks can be formed from accreting WDs (Baron et al. 1987; Nomoto & Kondo 1991; Woosley & Baron 1992; Fryer et al. 1999; Dessart et al. 2006; Abdikamalov et al. 2010; Mori et al. 2023; Longo Micchi et al. 2023). This channel is called accretion-induced collapse (AIC). Such NSs could be inside of globular clusters (Ivanova et al. 2008; Kremer et al. 2023). In our simulations, this channel is achieved from two paths. First, an oxygen-neon (ONe) WD increases its mass to the Chandrasekhar mass limit, accreting materials through mass transfer from its MS or post-MS (PMS) companion (non-degenerate companion). Second, two WDs merge without explosion. We describe the second path, since it is not implemented in previous BSE codes. We suppose that WD mergers create NSs under the following conditions.

- (i) The total mass of two WDs exceeds the Chandrasekhar mass limit.
- (ii) Neither of two WDs is a HeWD. Such WD merger products are thought to explode due to the double detonation scenario (Nomoto 1982; Woosley et al. 1986) in double WD systems (Perets et al. 2010; Guillochon et al. 2010; Pakmor et al. 2013, 2021; Shen et al. 2018; Tanikawa et al. 2018, 2019; Gronow et al. 2020; Ferrand et al. 2022; Zenati et al. 2023; El-Badry et al. 2023a).
- (iii) Both of two WDs do not consist of two carbon-oxygen (CO) WDs with  $\geq 0.8M_{\odot}$ . This type of merger products can experience explosion due to the violent merger scenario (Pakmor et al. 2010, 2011, 2012a,b). This condition is referred from Sato et al. (2015, 2016). Note that this criterion naturally includes an explosion due to the spiral instability (Kashyap et al. 2015).

These conditions are motivated by binary population synthesis modeling of type Ia SNe from WD mergers (Toonen et al. 2012; Ruiter 2019). We assume that two WD merger creates a NS with the following properties.

- (i) No natal kick. AIC develops only small asymmetry, similarly to an ECSN (Dessart et al. 2006; Schwab et al. 2015).
- (ii) The same mass as the total mass of the two WDs. WD mergers trigger nuclear reactions, however eject at most  $0.1M_{\odot}$  (Dan et al. 2014; Kashyap et al. 2018). Although the system can eject its mass during AIC, the ejecta mass is at most  $\sim 0.01M_{\odot}$  (Dessart et al. 2006; Mori et al. 2023; Longo Micchi et al. 2023). The total mass

**Table 1.** Summary of models. Parameters indicated by “–” are the same as those of the fiducial model.

Name	$M$ [ $M_\odot$ ]	$Z$	$\rho$ [ $M_\odot \text{pc}^{-3}$ ]	$f_{b,<5M_\odot}$	$\sigma_{k,\text{ccsn}}$ [ $\text{km s}^{-1}$ ]
Fiducial	1000	0.02	20	0.2	265
$M = 200M_\odot$	200	–	–	–	–
$M = 500M_\odot$	500	–	–	–	–
$M = 2000M_\odot$	2000	–	–	–	–
$Z = 0.01$	–	0.01	–	–	–
$Z = 0.005$	–	0.005	–	–	–
$Z = 0.002$	–	0.002	–	–	–
$Z = 0.0002$	–	0.0002	–	–	–
$\rho = 2$	–	–	2	–	–
$\rho = 200$	–	–	200	–	–
$f_{b,<5M_\odot} = 0$	–	–	–	0	–
$f_{b,<5M_\odot} = 0.5$	–	–	–	0.5	–
No-kick	–	0.002	–	–	0

of a WD merger product ( $\gtrsim 1.4M_\odot$ ) is larger than mass loss from the WD merger to AIC ( $\sim 0.1M_\odot$ ). Thus, we assume that the system loses no mass from the merger to AIC.

In Table 1, we summarize our cluster models. In the fiducial model, the initial cluster mass ( $M$ ) and stellar metallicity ( $Z$ ) are  $1000M_\odot$  and 0.02, respectively. A cluster is on a circular orbit at the distance of 8 kpc from the Galactic center. The initial cluster mass density  $\rho$  is  $20M_\odot \text{ pc}^{-3}$ , where  $\rho$  is defined as mass density inside the half-mass radius of a cluster. The initial binary fraction depends on primary star masses ( $m_1$ ). The initial binary fraction for  $m_1 \geq 5M_\odot$  ( $f_{b,\geq 5M_\odot}$ ) is unity (or 100 %), while the initial binary fraction for  $m_1 < 5M_\odot$  ( $f_{b,<5M_\odot}$ ) is 0.2. Note that the initial binary fraction is defined as  $N_b/(N_s + N_b)$ , where  $N_s$  and  $N_b$  are the numbers of single and binary stars, respectively. Single stars and primary stars in binaries have Kroupa’s initial mass function (Kroupa 2001) in the range from  $0.08M_\odot$  to  $150M_\odot$ . When the primary star of a binary has more than or equal to  $5M_\odot$ , the binary mass ratio ( $q$ ), orbital period ( $P$ ), and orbital eccentricity ( $e$ ) distributions are subject to initial conditions of Sana et al. (2012):  $f(q) \propto q^{-0.1}$  ( $0.1 \leq q \leq 1$ ),  $f(\log P) \propto (\log P)^{-0.55}$  ( $0.15 < \log(P/\text{day}) < 5.5$ ), and  $f(e) \propto e^{-0.42}$  ( $0 \leq e \leq 1$ ). When the primary star of a binary has less than  $5M_\odot$ , the binary mass ratio ( $q$ ), orbital period ( $P$ ), and orbital eccentricity ( $e$ ) distributions are subject to initial conditions of Kroupa (1995a,b) with modification of Belloni et al. (2017):  $f(q) \propto \text{const}$ ,  $f(\log P) \propto (\log(P/\text{day}) - 1)/(45 + [\log(P/\text{day}) - 1]^2)$  ( $10 \leq P/\text{day} \leq 10^{8.43}$ ), and  $f(e) \propto e$ . We make these initial conditions by means of MCLUSTER (Küpper et al. 2011). The simulations are finished at 1 Gyr.

We prepare cluster models in which one parameter is different from those in the fiducial model. The  $M = 200M_\odot$ ,  $M = 500M_\odot$  and  $M = 2000M_\odot$  models have clusters with the initial masses of  $200M_\odot$ ,  $500M_\odot$  and  $2000M_\odot$ , respectively. The  $Z = 0.01$ ,  $Z = 0.005$ ,  $Z = 0.002$ , and  $Z = 0.0002$  models have clusters with stellar metallicities of  $Z = 0.01$ ,  $0.005$ ,  $0.002$ , and  $0.0002$  respectively. The  $\rho = 2$  and  $\rho = 200$  models have clusters with the initial mass densities of 2 and  $200M_\odot \text{ pc}^{-3}$ , respectively. The  $f_{b,<5M_\odot} = 0$  and  $f_{b,<5M_\odot} = 0.5$  models have  $f_{b,<5M_\odot} = 0$  and 0.5, respectively. Note that  $f_{b,\geq 5M_\odot}$  is fixed to unity, which is reasonable according to Sana et al. (2012) and Moe & Di Stefano (2017).

Additionally, we make the no-kick model in which no CCSNe generate kick velocities, in order to investigate effects of CCSN natal kicks. We set the metallicity to  $Z = 0.002$ , because the visible star

of Gaia NS1 has small metallicity,  $[\text{Fe}/\text{H}] = -1.23$  (El-Badry et al. 2024).

We generate a large number of open clusters with different realizations, so that each model contains  $10^7 M_\odot$  open clusters in total. The total mass of simulated clusters is  $1.3 \times 10^8 M_\odot$ . We can expect that we obtain  $\sim 100$  Gaia BHs from each cluster model, because the formation efficiency of Gaia BHs is  $\sim 10^{-6} M_\odot^{-1}$  (Rastello et al. 2023; Di Carlo et al. 2023; Tanikawa et al. 2024). This enables us to make comparison between the formation efficiencies of Gaia BHs and NSs.

From our simulations, we pick up compact binaries with the following criteria:

(i)  $10^2 \leq P/\text{day} \leq 10^4$ , where  $P$  is a binary orbital period. This criterion may look loose, since the orbital periods of Gaia BH1, BH2, and NS1 are 180, 1300, and 730 days, respectively. Thus, we also investigate the case for  $10^2 \leq P/\text{day} \leq 10^3$ .

(ii)  $m_2 \leq 1.1M_\odot$ , where  $m_2$  is a companion mass. This is because Gaia BH1, BH2, and NS1 have light companion stars: 0.93, 1.07, and  $0.79M_\odot$ , respectively.

(iii) Located outside of open clusters. None of Gaia BH1, BH2 and NS1 are located in open clusters.

Note that we do not put any constraints on orbital eccentricities in the above criteria. On the other hand, Gaia BHs and NS1 are characterized by moderately high eccentricities ( $\sim 0.5$ ) and small (but non-zero) eccentricity ( $\sim 0.1$ ), respectively. Compact binaries we pick up may not be necessarily identified as Gaia BHs and NSs. Thus, these compact binaries are hereafter called “inert compact binaries”. They are also called “inert BH binaries (inert BHBs)” and “inert NS binaries (inert NSBs)” if they contain BHs and NSs, respectively.

### 3 RESULTS

First, We make clear whether inert BHBs and NSBs are formed from primordial binaries, or not. We find that no inert BHBs nor NSBs originate from primordial binaries in all our models other than the no-kick model. In the no-kick model, no inert BHBs originate from primordial binaries, while inert NSBs can be formed from primordial binaries and through dynamical interactions. Dynamical interactions play an important role in forming inert BHBs regardless of the presence of CCSN natal kicks. On the other hand, the formation of inert NSBs strongly depend on CCSN natal kicks. In section 3.1, we first investigate simulation results of models with CCSN natal kicks. In section 3.2, we compare simulation results of models with and without CCSN natal kicks.

#### 3.1 Standard CCSN natal kicks

Figure 1 shows the formation efficiencies of inert BHBs and NSBs in all our cluster models other than the no-kick model. Inert BHBs with  $10^2 \leq P/\text{day} \leq 10^4$  are formed at a formation efficiency of  $10^{-6}$ – $10^{-5} M_\odot^{-1}$  except for the  $f_{b,<5M_\odot} = 0$  model. This is consistent with previous results (Di Carlo et al. 2023; Rastello et al. 2023; Tanikawa et al. 2024). The formation efficiencies slowly increase with metallicity decreasing, initial cluster mass increasing, and initial half-mass density increasing. This is because more metal-poor, larger-mass, and higher-density clusters are harder to be disrupted in the Galactic tidal field, and thus these clusters have longer time to form inert BHBs. The formation efficiency in the  $f_{b,<5M_\odot} = 0$  model is much smaller than those in the other models for the following reason.

**Table 2.** P-values of the Kolmogorov-Smirnov (K-S) test for eccentricity distributions of inert BHBs and NSBs.

Binary type	Number	Comparison	P-value
Inert BHB ( $10^2$ - $10^4$ day)	556	Thermal	$5.6 \times 10^{-5}$
Inert BHB ( $10^2$ - $10^3$ day)	97	Thermal	$9.3 \times 10^{-2}$
Inert NSB ( $10^2$ - $10^4$ day)	6	Thermal	$4.2 \times 10^{-2}$
Inert NSB selected	4	Thermal	$1.4 \times 10^{-1}$
Inert NSB (no-kick)	34	Thermal	$2.5 \times 10^{-3}$
Inert BHB ( $10^2$ - $10^4$ day)	556	Gaia BHs	$2.4 \times 10^{-1}$
Inert BHB ( $10^2$ - $10^3$ day)	97	Gaia BHs	$2.7 \times 10^{-1}$
Inert NSB ( $10^2$ - $10^4$ day)	6	Gaia NS1	$2.9 \times 10^{-1}$
Inert NSB selected	4	Gaia NS1	$4.0 \times 10^{-1}$
Inert NSB (no-kick)	34	Gaia NS1	$5.7 \times 10^{-2}$

Generally, an inert BHB is formed, such that a single BH captures one star in a binary. Since the number of binaries in the  $f_{b, < 5M_\odot} = 0$  model is much smaller than those in the other models, inert BHBs are harder to form in the  $f_{b, < 5M_\odot} = 0$  model. Nevertheless, it is worth remarking that inert BHBs are formed at an efficiency of  $\sim 10^{-7} M_\odot^{-1}$  even in the  $f_{b, < 5M_\odot} = 0$  model. They would be formed through triple-single encounters. This indicates that inert BHBs are robustly formed in open clusters, even if an initial binary fraction is extremely low. This is consistent with the results of [Tanikawa et al. \(2024\)](#).

Inert BHBs for  $10^2 \leq P/\text{day} \leq 10^3$  are formed at an efficiency of  $10^{-7}$ - $10^{-6} M_\odot^{-1}$ . In the  $M = 2000M_\odot$  and  $\rho = 200$  models, the number ratio of such inert BHBs to all inert BHBs is large, more than 0.1. This would be because these clusters have larger escape velocities than the other models. A cluster with a larger escape velocity can retain closer binaries kicked by their dynamical interactions, and so make them closer and closer. Although the number ratio is also large in the  $f_{b, < 5M_\odot} = 0$  model, we cannot identify if it is real, because the number of inert BHBs is too small.

In contrast to inert BHBs, inert NSBs are hardly formed. The number of inert NSBs is only 6 even if we put together all the models. It is only 3 for inert NSBs with  $10^2 \leq P/\text{day} \leq 10^3$ . If we weigh equally all the models, the formation efficiency is  $6 \times 10^{-8} M_\odot^{-1}$  for all the inert NSBs, and  $3 \times 10^{-8} M_\odot^{-1}$  for inert NSBs with  $10^2 \leq P/\text{day} \leq 10^3$ . The formation efficiency of inert NSBs is smaller than that of inert BHBs by at least an order of magnitude.

Figure 2 shows the orbital eccentricity distribution of inert BHBs and NSBs. We put together inert BHBs and NSBs among all the models other than the no-kick model. We have to put together inert NSBs, because the number of inert NSBs is too small to statistically investigate the eccentricity distribution of inert NSBs for each model. We adopt the Kolmogorov-Smirnov (K-S) test to compare these distribution with the thermal distribution ([Heggie 1975](#)) and Gaia BHs and NSs. Note that Gaia BH1, BH2 and NS1 have orbital eccentricities of  $\sim 0.451$  ([El-Badry et al. 2023b](#)), 0.518 ([El-Badry et al. 2023c](#)), and 0.124 ([El-Badry et al. 2024](#)), respectively. Table 2 shows the P-values of the K-S test. The eccentricity distribution of inert BHBs with  $10^2 \leq P/\text{day} \leq 10^4$  is clearly more circular than the thermal distribution, since the P-value is  $5.6 \times 10^{-5}$ . This is possibly because eccentric BHBs are circularized by tidal interactions. This is also seen in the eccentricity-period diagram of binaries in Gaia DR3 (e.g. [Gaia Collaboration et al. 2023b](#)). On the other hand, the eccentricity distribution of inert BHBs with  $10^2 \leq P/\text{day} \leq 10^3$  is not significantly different from the thermal distribution; the P-value is  $9.3 \times 10^{-2}$ . This may be due to their small number.

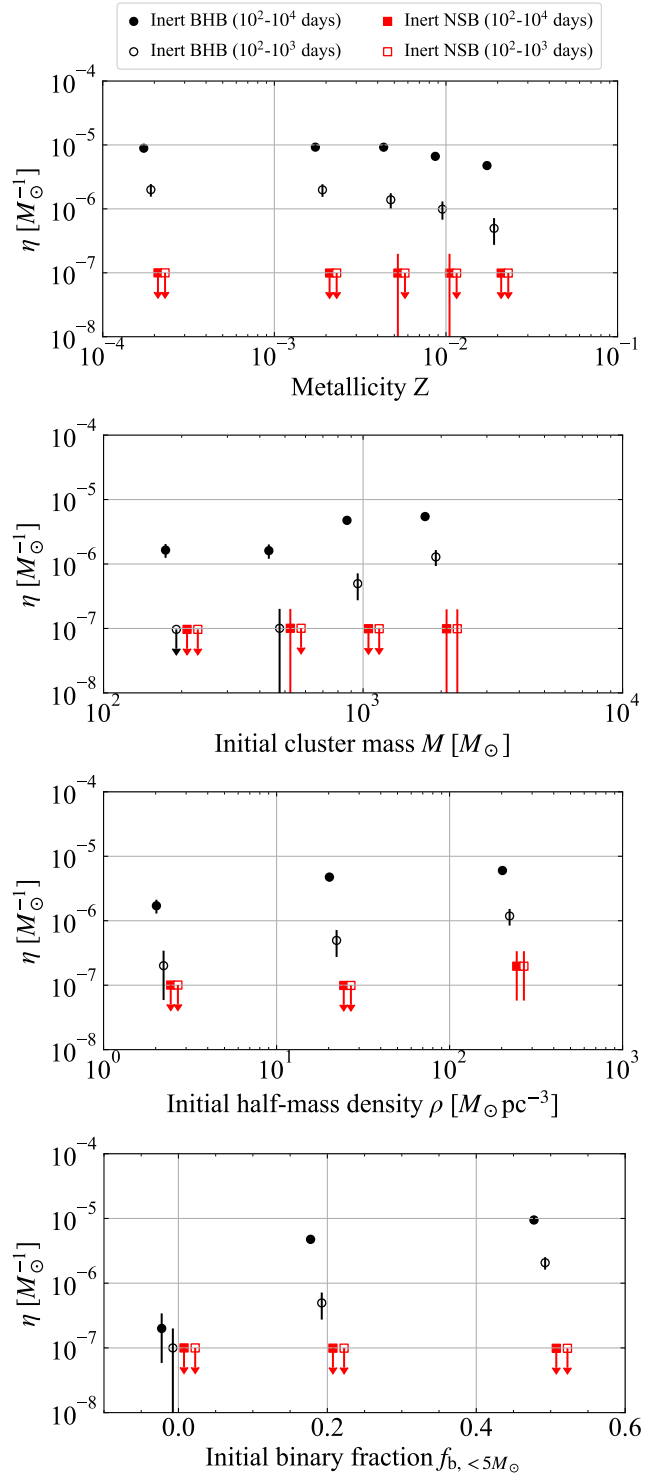


**Figure 1.** Formation efficiencies of inert BHBs (circles) and NSBs (squares) as a function of metallicity ( $Z$ ), initial cluster mass ( $M$ ), initial half-mass density ( $\rho$ ), and initial binary fraction ( $f_{b, < 5M_\odot}$ ). Filled and open points show that the ranges of binary orbital periods are  $10^2$ - $10^4$  days and  $10^2$ - $10^3$  days, respectively. Circles and squares indicate inert BHBs and NSBs, respectively. These points are slightly shifted leftward or rightward for visibility. We calculate error bars, assuming that inert BHBs and NSBs are formed in Poisson process. Error bars in some models reach zero, since only one inert BHB or NSB is formed in these models. In several models, no inert NSBs are formed. For these models, we use down arrows to indicate the upper limits of inert NSB formation efficiencies.

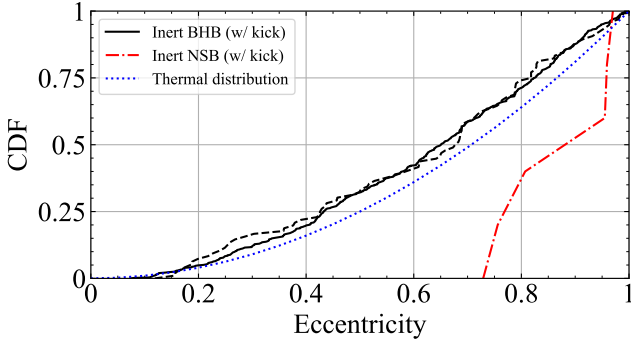


**Figure 2.** Cumulative eccentricity distribution of inert BHBs and NSBs. Solid and dashed curves indicate inert BHBs with binary orbital periods of  $10^2$ - $10^4$  and  $10^2$ - $10^3$  days, respectively. The dot dashed curve indicates inert NSBs in all the models. The dotted curve shows the thermal distribution.

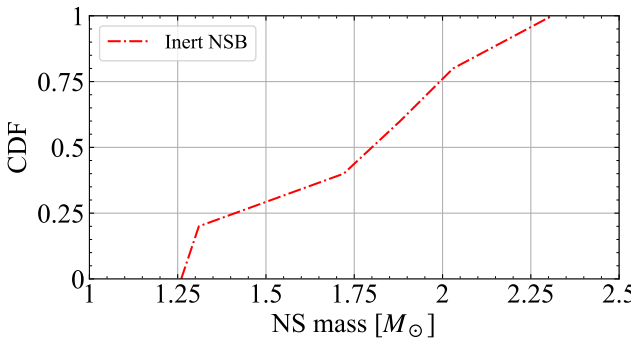
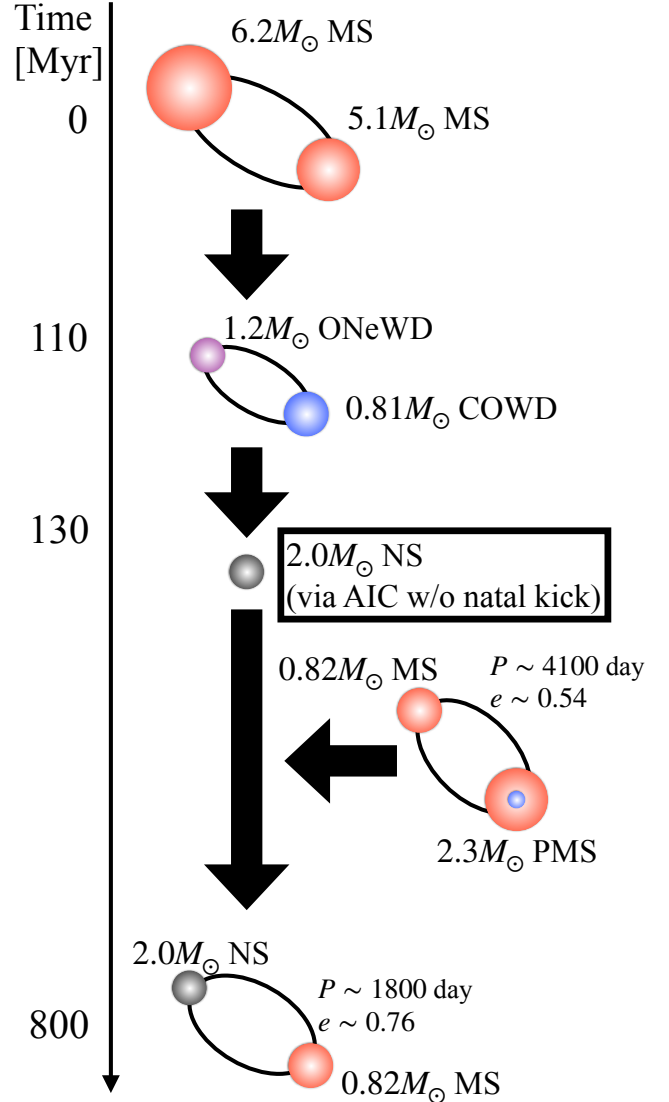


**Figure 3.** Cumulative NS mass distribution of inert NSBs in all the models.

Although the eccentricity distribution of inert NSBs appears to be largely different from the thermal distribution, it is still consistent with the thermal distribution. The P-value is not small:  $4.2 \times 10^{-2}$ . This may be again due to the small statistics. As described later, the inert NSBs with the highest and second highest eccentricities are not formed through dynamical interactions (named “CCSN channel” later), although they are not primordial binaries. Moreover, these inert NSBs are formed only in the  $\rho = 200$  model. A large fraction of open clusters in reality could be less dense than the  $\rho = 200$  model. Thus, we construct inert NSBs, excluding these NSBs (“inert NSB selected” in Table 2). When we compare their eccentricity distribution with the thermal distribution, the P-value increases to  $1.4 \times 10^{-1}$ . It is natural that they are formed through dynamical interactions. Nevertheless, their eccentricity distribution may finally becomes more circular than the thermal distribution, similarly to inert BHBs, if we obtain more many inert NSBs with simulating more many clusters.

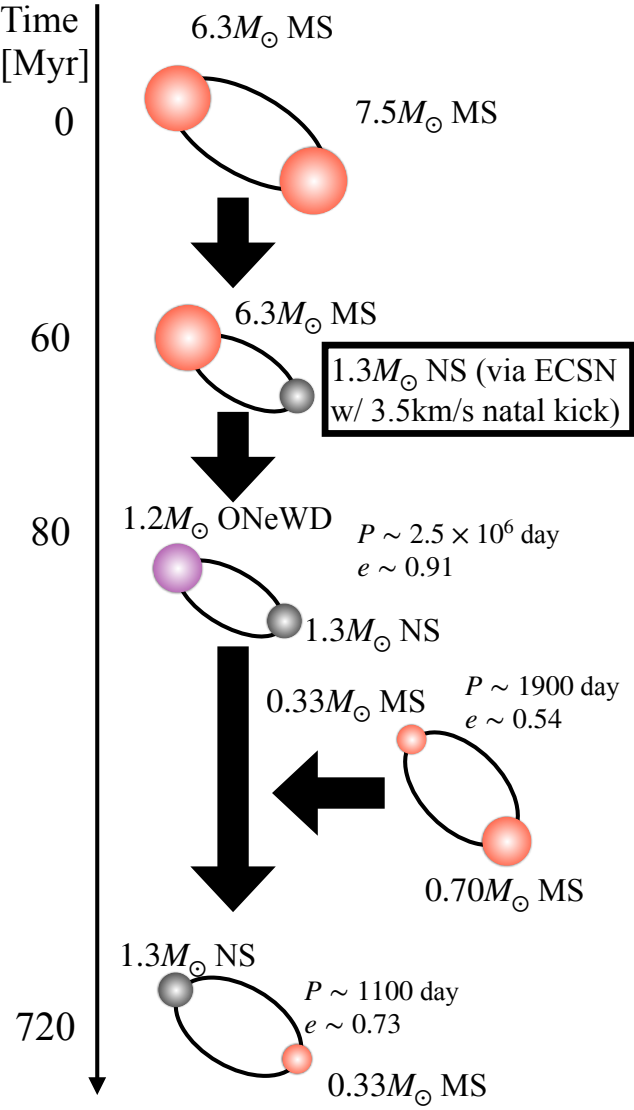
Inert BHBs and NSBs have the eccentricity distributions which are not inconsistent with Gaia BHs and NSs, respectively, regardless of how to choose these BHBs and NSBs. The P-values are more than 0.1. This may be due to the small numbers; the number of inert NSBs are only 6, and the numbers of Gaia BHs and NSs are 2 and 1, respectively. It seems that the eccentricity distributions are not currently helpful to assess if inert BHBs and NSBs are identified as Gaia BHs and NSs, respectively.

Figure 3 shows the NS mass distribution of all the inert NSBs. 2 of the 6 inert NSBs have NSs with  $> 2M_\odot$ . These NSs are formed through AIC of WD merger products (called “AIC channel” later). The detail formation channel is described below.



**Figure 4.** Inert NSB formation channel via AIC. This happens in model  $Z = 0.005$ . A binary with  $6.2$  and  $5.1M_\odot$  MSs evolves to binary WDs with  $1.2M_\odot$  ONeWD and  $0.81M_\odot$  COWD. These WDs merge, and its merger product collapses to a NS. Because this NS receives no natal kick, it stays inside of the open cluster. The NS closely interacts with a binary with  $0.82M_\odot$  MS and  $2.3M_\odot$  PMS, and capture the  $0.82M_\odot$  MS, resulting in an inert NSB. It finally escapes from the open cluster.

Hereafter, we describe three formation channels of inert NSBs. These channels are illustrated in Figures 4, 5, and 6. In the first channel, NSs are formed through AIC of WD merger products. We call this channel “AIC channel”. We explain the AIC channel along with Figure 4. This channel starts with a primordial binary consisting of intermediate mass stars:  $6.2$  and  $5.1M_\odot$  MSs. They evolve to a close double WDs with  $1.2M_\odot$  ONeWD and  $0.81M_\odot$  COWD via common envelope evolution. They merge through orbital decay due to gravitational wave radiation. The merger product avoids type Ia SN explosion, and collapses to a NS (AIC). The NS mass is  $> 2M_\odot$ . The NS can avoid escaping from the open cluster, since AIC generate no natal kick in our model. Finally, the NS dynamically interacts with another primordial binary, and captures one star of the primordial binary. The resulting NSB has orbital period and eccentricity of



**Figure 5.** Inert NSB formation channel via ECSN. This happens in model  $Z = 0.01$ . A binary with  $7.5$  and  $6.3 M_{\odot}$  MSs evolves to a binary with  $1.3 M_{\odot}$  NS and  $1.2 M_{\odot}$  ONeWD. The NS receives a small kick ( $3.5 \text{ km s}^{-1}$ ) because of ECSN, and is retained in the open cluster. The binary interacts with a binary with  $0.70$  and  $0.33 M_{\odot}$  MSs, and leaves an inert NSB consisting of the NS and  $0.33 M_{\odot}$  MS. The inert NSB finally escapes from the open cluster.

$\sim 1800$  day and  $\sim 0.76$ , respectively. This happens in the  $Z = 0.005$  model. Another one also occurs in the  $M = 2000 M_{\odot}$  model.

Our simulations implement a NS formation channel through AIC of WDs accreting from non-degenerate companions. In fact, we find such NS formations. However, they do not evolve to inert NSBs. Their orbital periods are much shorter than  $10^2$  days, because such NS formations involve mass transfer from non-degenerate companions. These binaries are too close to interact with other stars dynamically. Moreover, if they experience dynamical interactions, their orbital periods will be still much shorter than  $10^2$  days. Such tight binaries tend to become tighter through dynamical interactions.

The second channel involves ECSNe as seen in Figure 5. We call this channel ‘‘ECSN channel’’. We find this channel in the  $Z = 0.01$  and  $M = 500 M_{\odot}$  models. Here, we introduce the formation processes of the inert NSB in the former model (see also Figure 5). A  $7.5 M_{\odot}$

MS with a  $6.3 M_{\odot}$  MS companion evolves to a  $1.3 M_{\odot}$  NS via ECSN. Because of ECSN, the NS receives a small kick velocity ( $3.5 \text{ km s}^{-1}$ ), and is not ejected from the open cluster. Its companion evolves to a  $1.2 M_{\odot}$  ONeWD. This binary experiences no interaction any more, since their separation is large. Very later, this binary interacts with another binary with  $0.33$  and  $0.70 M_{\odot}$  MSs. This interaction raises an inert NSB with the  $1.3 M_{\odot}$  NS and  $0.33 M_{\odot}$  MS. Note that, although a lower-mass star is harder to be took as a binary member, it is not impossible. This has orbital period and eccentricity of  $\sim 1100$  day and  $0.73$ , respectively.

In the third channel, NSs arise from CCSNe. Thus, we refer to them as ‘‘CCSN channel’’. We obtain two inert NSBs, both of which are formed in the  $\rho = 200$  model. In Figure 6, we show the formation pathway of one of the two. This channel begins with a primordial binary with  $18$  and  $17 M_{\odot}$  MSs. The primordial binary merges to a  $35 M_{\odot}$  MS. Just after the merger, the  $35 M_{\odot}$  MS soon captures a  $0.75 M_{\odot}$  MS. It evolves to a  $32 M_{\odot}$  PMS, and experiences common envelope evolution with its  $0.75 M_{\odot}$  MS companion. The common envelope evolution leaves a short-period (2.8 day) binary with a  $6.8 M_{\odot}$  He star and  $0.75 M_{\odot}$  MS. The He star causes a CCSN with a kick velocity of  $260 \text{ km s}^{-1}$ . It luckily survives as a binary. Such a close binary can survive a CCSN depending on the kick velocity direction despite of CCSN mass loss, because its binary internal motion has large velocity comparable to the kick velocity. However, the natal kick greatly affects the center-of-mass velocity of the binary, and ejects the resulting NSB from the open cluster.

The CCSN channel involves a dynamical interaction to form the progenitors of inert NSBs, while the final configurations of inert NSBs are dependent on binary physics, not on dynamical interactions. Furthermore, this channel tends to inert NSBs with high eccentricities. In fact, the two NSBs formed through the CCSN channel have the highest and second highest eccentricities among inert NSBs in all our models other than the no-kick model. Thus, we exclude inert NSBs via the CCSN channel from the ‘‘inert NSBs selected’’ in Table 2 when we compare their eccentricity distribution with the thermal distribution.

The CCSN channel appears only in the  $\rho = 200$  model. We interpret the reason as follows. This channel requires a post common envelope binary consisting of  $\leq 1.1 M_{\odot}$  MS star and massive He star (say  $\gtrsim 3 M_{\odot}$ ). If a He star has  $\lesssim 3 M_{\odot}$ , such a post common envelope binary cannot become wide enough to be an inert NSB after the He star collapses to a NS. This is because the He star does not lose its mass during its CCSN. The kick velocity is at most comparable to the velocity of the binary internal motion, and thus cannot change the binary period largely. A He star with  $\gtrsim 3 M_{\odot}$  is raised by a  $\gtrsim 11 M_{\odot}$  MS. However, our initial conditions prohibit primordial binaries with  $\gtrsim 11 M_{\odot}$  and  $\lesssim 1.1 M_{\odot}$  MS stars, since the minimum binary mass ratio is 0.1. Thus, binaries with  $\gtrsim 11 M_{\odot}$  and  $\lesssim 1.1 M_{\odot}$  MS stars need to be formed through dynamical interactions before  $\gtrsim 11 M_{\odot}$  stars evolve to NSs or BHs. Dynamical interactions in the  $\rho = 200$  model are the most active among all our models because of its high density. Thus, many binaries with  $\gtrsim 11 M_{\odot}$  and  $\lesssim 1.1 M_{\odot}$  MS stars are formed, and there are many chances to achieve the CCSN channel in the  $\rho = 200$  model. We have to note that this reason strongly depends on our initial conditions in which there are no primordial binaries with  $\gtrsim 11 M_{\odot}$  and  $\lesssim 1.1 M_{\odot}$  MS stars. It would not be strange if The CCSN channel is achieved in real open clusters with the initial half-mass density of  $< 200 M_{\odot} \text{ pc}^{-3}$ .

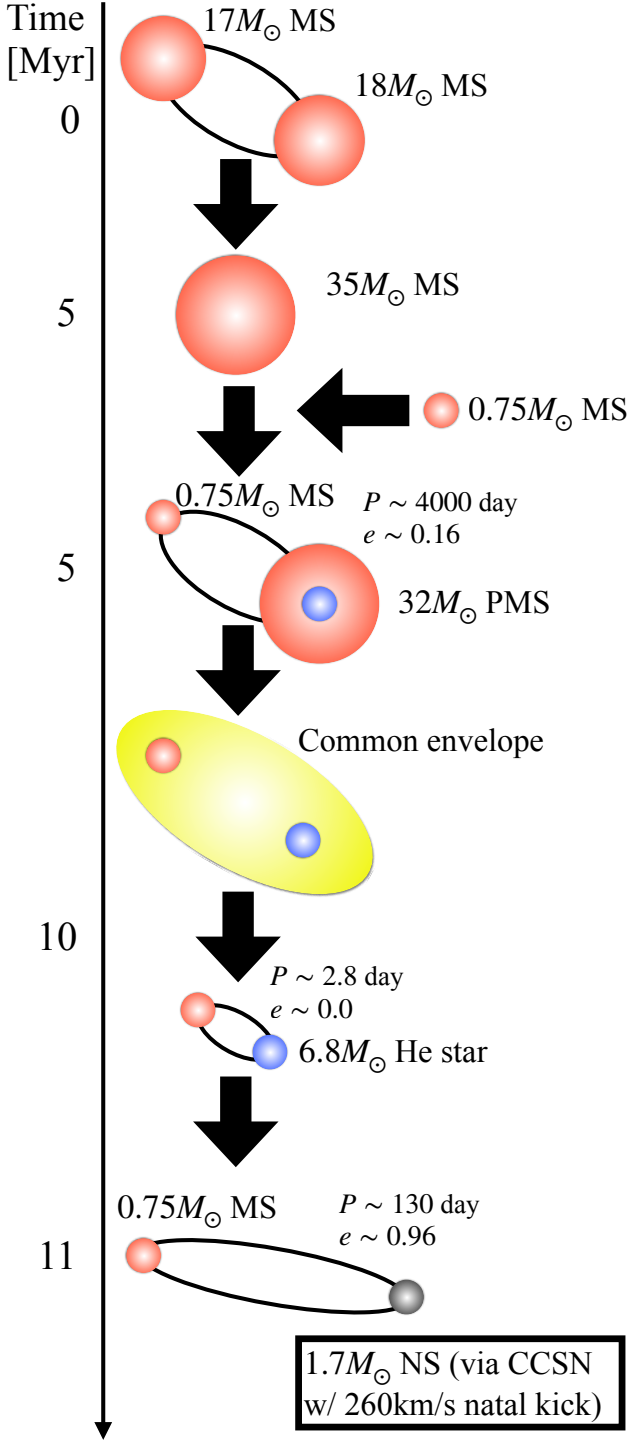


**Figure 6.** Inert NSB formation channel via CCSN. This happens in model  $\rho = 200$ . A binary with 18 and  $17M_{\odot}$  MSs merges to a  $35M_{\odot}$  MS. The  $35M_{\odot}$  MS soon captures a  $0.75M_{\odot}$  MS. This binary experiences common envelope evolution, and results in a close binary with a  $6.8M_{\odot}$  He star and a  $0.75M_{\odot}$  MS. The He star undergoes CCSN, and creates a  $1.7M_{\odot}$  NS. Although the NS receives a large kick ( $260 \text{ km s}^{-1}$ ), the binary is not disrupted because of the close separation, and becomes an inert NSB. On the other hand, the large kick ejects the inert NSB from the open cluster.

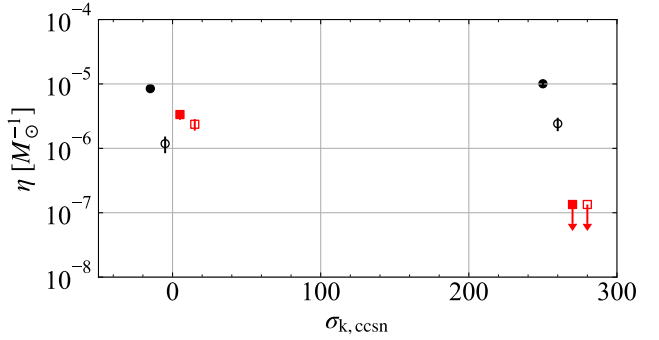


**Figure 7.** The same as Figure 1 except for a function of CCSN natal kick velocity ( $\sigma_{k,ccsn}$ ). The results of  $Z = 0.002$  and no-kick models are shown.

### 3.2 Effects of CCSN natal kicks

Hereafter, we investigate the effects of CCSN natal kicks, showing the simulation results of the no-kick model. Figure 7 shows the formation efficiency of inert BHBs and NSBs in the  $Z = 0.002$  and no-kick models. The formation efficiency of inert BHBs in the no-kick model is similar to that in the other models regardless of  $10^2 \leq P/\text{day} \leq 10^4$  and  $10^2 \leq P/\text{day} \leq 10^3$ . On the other hand, NSBs are formed much more efficiently in the no-kick model (a few  $10^{-6} M_{\odot}^{-1}$ ) than in the other models ( $\lesssim 10^{-7} M_{\odot}^{-1}$ ). There are 34 inert NSBs with  $10^2 \leq P/\text{day} \leq 10^4$ . 25 of them originate from primordial binaries, and the rest of them are formed through dynamical interactions.

The no-kick model has a high formation efficiency of inert NSBs, in contrast to other models. As described above, a dominant fraction of inert NSBs ( $\sim 70\%$ ) originate from primordial binaries. We describe their formation pathway here. We do not illustrate it, because we suppose the no-kick model is unrealistic. Let's prepare a binary with  $\sim 8M_{\odot}$  and  $\sim 1M_{\odot}$  MSs. Its separation is  $\sim 3 \times 10^3 R_{\odot}$ . The heavier star evolves to a PMS, and fills its Roche lobe. Then, the binary experiences common envelope evolution. The common envelope evolution leaves a binary with  $\sim 2M_{\odot}$  He star and  $\sim 1M_{\odot}$  MS star. It is separated by  $\sim 40R_{\odot}$ . The He star causes a CCSN, and leaves behind a NS. Because of CCSN mass loss, the binary is widened, and fits in an inert NSB. In all the models with CCSN natal kicks, such inert NSBs cannot be formed. CCSN natal kicks disrupt the binary at a high probability. Just before CCSNe, the velocities of binary internal motions have  $\sim 100 \text{ km s}^{-1}$ , much smaller than CCSN natal kick velocities ( $265 \text{ km s}^{-1}$ ).

9 of 34 inert NSBs are dynamically formed. For 6 of them, NSs capture their companions. On the other hand, for the rest of them, NS progenitors capture their companions, and later they collapse to NSs. The latter formation pathway is the same as the formation pathway from primordial binaries described above, except that a binary with  $\sim 8M_{\odot}$  and  $\sim 1M_{\odot}$  MSs is formed through dynamical interactions.

Figure 8 shows the cumulative eccentricity distribution of inert NSBs in the no-kick model. Their orbital eccentricities appear to deviate from the thermal distribution. In fact, the deviation is significant; the P-value of the K-S test is  $2.5 \times 10^{-3}$  as seen in Table 2. This is because a dominant fraction of these inert NSBs originate from primordial binaries, not formed through dynamical interactions. On the other hand, the eccentricity distribution of these NSBs is not significantly different from Gaia NS1; the P-value is  $5.7 \times 10^{-2}$ . This shows that it is difficult to distinguish the differences among these eccentricity distributions due to the small statistics.

When we switch off CCSN natal kicks, the number of NSs retained

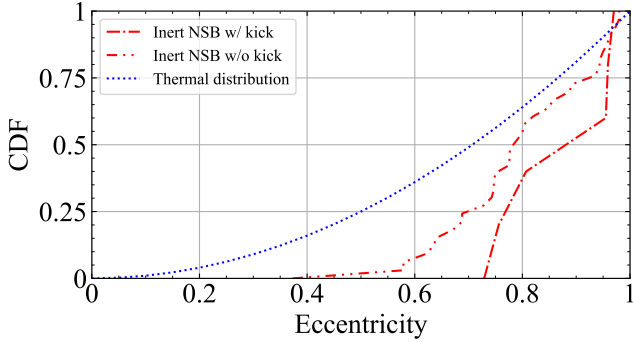


**Figure 8.** Cumulative eccentricity distribution of inert NSBs in all models except for the no-kick model (Inert NSB w/ kick), and in the no-kick model (Inert NSB w/o kick). The dotted curve shows the thermal distribution.

in open clusters should increase by about 100 times. Nevertheless, the number of inert NSBs dynamically formed is still low for the following reason. NSs are hard to capture other stars dynamically, because their masses are comparable to or less than surrounding main-sequence (MS) stars. Note that the lifetime of a  $1.4M_{\odot}$  MS star is a few Gyr, which is longer than the lifetime of open clusters.

#### 4 DISCUSSION

First, we discuss whether inert BHBs and NSBs correspond to Gaia BHs and NSs, respectively. Here, we do not consider the simulation results of the no-kick model. As seen in Table 2, the P-values of the K-S test do not show that inert BHBs have different orbital eccentricities from Gaia BHs. The eccentricity distributions of inert NSBs with  $10^2 \leq P/\text{day} \leq 10^4$  and inert NSBs selected in Table 2 are not inconsistent with Gaia NS1's eccentricity.

Indeed, only Gaia NS1's orbital elements have been publicly reported among Gaia NSs, and moreover we do not obtain a sufficient number of inert NSBs from our simulations. Only based on their orbital eccentricities, we cannot robustly conclude if Gaia NS1 is formed in open clusters, or not. Here, we compare the formation efficiencies of inert BHBs and NSBs, assuming that inert NSBs correspond to Gaia NSs. The formation efficiency of inert NSBs is smaller than that of inert BHBs by two or more orders of magnitude except for the no-kick model (see Figure 1). However, the number of discovered Gaia NSs, 20 (El-Badry et al. 2024), is much larger than the number of Gaia BHs, 2. This shows that open clusters cannot form enough Gaia NSs to be already discovered.

This is also true for the no-kick model. As for inert BHBs and NSBs with  $10^2 \leq P/\text{day} \leq 10^4$ , the formation efficiency of inert NSBs is smaller than that of inert BHBs. Actually, the formation efficiency of inert NSBs with  $10^2 \leq P/\text{day} \leq 10^3$  is larger than that of inert BHBs with  $10^2 \leq P/\text{day} \leq 10^3$ . However, a dominant fraction of inert NSB formed in the no-kick model ( $\sim 74\%$ ) originate from primordial binaries. This means that such inert NSBs can be formed through isolated binary evolution if CCSN natal kicks are smaller than expected. In this case, although a large number of inert NSBs can be formed in open clusters, inert NSBs are also formed more efficiently on isolated fields. Thus, open clusters cannot dominate the formation of Gaia NSs, even if CCSN natal kicks are unrealistically small.

It is unclear how efficiently Gaia (Gaia Collaboration et al. 2023b) and its spectroscopic follow-up observations (El-Badry et al. 2023b,c, 2024; Chakrabarti et al. 2023) can discover Gaia BHs and NSs. Thus,

the numbers of discovered Gaia BHs and NSs do not directly mean their intrinsic numbers. However, for the following reason, we infer that Gaia NSs are harder to be discovered than Gaia BHs, and that the intrinsic number of Gaia NSs should be much larger than that of Gaia BHs. All Gaia and its follow-up observations search for Gaia BHs and NSs, observing BHs' and NSs' companions. Because such companions are swayed more largely with BH and NS masses increasing, Gaia, astrometric observations, can more easily discover BHs and NSs with larger masses. Similarly, companions tend to have larger radial velocity variations, and thus spectroscopic follow-up observations can detect more massive BHs and NSs more efficiently. Since NSs are generally less massive than BHs, the intrinsic number ratio of Gaia NSs to Gaia BHs should be larger than the reported number ratio. As seen in section 3, open clusters form Gaia BHs more efficiently than Gaia NSs. This is in contrast to the observational results. Eventually, open clusters cannot form both of Gaia BHs and Gaia NSs.

As described above, Gaia NSs are unlikely to be formed in open clusters. Nevertheless, we do not mean that Gaia BHs are not formed in open clusters. The formation efficiency of Gaia BHs in  $\sim 10^3 M_{\odot}$  open clusters is still high ( $\sim 10^{-6}$ - $10^{-5} M_{\odot}$ ), if we do not adopt unrealistically small half-mass density ( $\rho \sim 2 M_{\odot} \text{ pc}^{-3}$ ) nor unrealistically small binary fraction ( $f_{\text{b},<5M_{\odot}} \sim 0$ ). It is reasonable that open clusters have  $\rho \gtrsim 20 M_{\odot} \text{ pc}^{-3}$  initially. Note that, although nearby open clusters have  $\rho \sim 10^{-2}$ - $10^{-2} M_{\odot} \text{ pc}^{-3}$ , they should become less dense with time through gas expulsion, stellar evolution mass loss, and two-body relaxation (Portegies Zwart et al. 2010). Initial binary fractions in open clusters should be  $f_{\text{b},<5M_{\odot}} \gtrsim 0.2$ , similarly to isolated fields (Sana et al. 2012; Moe & Di Stefano 2017). It would be possible that Gaia BHs are formed in open clusters, while Gaia NSs (El-Badry et al. 2024) and ultramassive WDs (Yamaguchi et al. 2024) are formed on isolated fields. This will become clear after much more Gaia BHs and NSs will be discovered.

#### 5 SUMMARY

We have performed gravitational  $N$ -body simulations for  $1.3 \times 10^8 M_{\odot}$  open clusters in total with various masses, metallicities, densities, binary fractions, and natal kick velocities. We have found that the formation efficiency is  $10^{-6}$ - $10^{-5} M_{\odot}^{-1}$  for Gaia BHs in open clusters with realistic parameters, while  $\lesssim 10^{-7} M_{\odot}^{-1}$  for Gaia NSs. This is in contrast to observational results in which the number of discovered Gaia BHs (2) is smaller than that of Gaia NSs ( $\sim 20$ ). On the other hand, inert BHBs and NSBs obtained from our simulations have orbital eccentricities not inconsistent with Gaia BHs and NSs, respectively. This is partly because of the small statistics for Gaia BHs and NSs, where only one Gaia NS's orbital elements are publicly available.

We have switched off CCSN natal kicks in order to increase the number of NSs retained in open clusters. Although we expected the number of inert NSBs to increase, the formation efficiency of inert NSBs is at most comparable to that of inert BHBs. NSs are much harder to capture companions than BHs, since NSs are not so heavier than MSs and WDs during open cluster lifetimes ( $\sim 1$  Gyr). Moreover, a dominant fraction of them are formed from primordial binaries. Thus, inert NSBs are less efficiently formed in open clusters than on isolated fields, even if CCSNe generate no natal kicks.

Regardless of the presence and absence of CCSN natal kicks, inert NSBs are formed in open clusters less efficiently than, or at most comparable to inert BHBs. Additionally, if there are no CCSN natal kicks, inert NSBs are formed more efficiently on isolated fields than

in open clusters. Thus, we have concluded that open clusters cannot form both Gaia BHs and NSs. However, we do not mean that open clusters cannot form Gaia BHs. It would be possible that Gaia BHs are formed in open clusters, while Gaia NSs are formed on isolated fields. We will make it clear when more many Gaia BHs and NSs will be discovered in the future.

## ACKNOWLEDGMENTS

This research could not be accomplished without the support by Grants-in-Aid for Scientific Research (19K03907) from the Japan Society for the Promotion of Science. M.F. is supported by The University of Tokyo Excellent Young Researcher Program. L.W. thanks the support from the one-hundred-talent project of Sun Yat-sen University, the Fundamental Research Funds for the Central Universities, Sun Yat-sen University (22hytd09) and the National Natural Science Foundation of China through grant 12073090 and 12233013. Numerical simulations are carried out on Small Parallel Computers at Center for Computational Astrophysics, National Astronomical Observatory of Japan, the Yukawa Institute Computer Facility, and Cygnus/Pegasus at the CCS, University of Tsukuba.

## DATA AVAILABILITY

Results will be shared on reasonable request to authors. The data is generated by the software PeTar and SDAR, which are available in GitHub at <https://github.com/lwang-astro/PeTar> and <https://github.com/lwang-astro/SDAR>, respectively. The initial conditions of star cluster models are generated by the software MCLUSTER (Küpper et al. 2011), which is available in GitHub at <https://github.com/lwang-astro/mcluster>.

## REFERENCES

Abbott B. P., et al., 2019, *Physical Review X*, **9**, 031040  
 Abbott R., et al., 2021, *Physical Review X*, **11**, 021053  
 Abbott R., et al., 2023, *Physical Review X*, **13**, 011048  
 Abdikamalov E. B., Ott C. D., Rezzolla L., Dessart L., Dimmelmeier H., Marek A., Janka H. T., 2010, *Phys. Rev. D*, **81**, 044012  
 Abdul-Masih M., et al., 2020, *Nature*, **580**, E11  
 Andrews J. J., Taggart K., Foley R., 2022, arXiv e-prints, p. [arXiv:2207.00680](https://arxiv.org/abs/2207.00680)  
 Banerjee S., Belczynski K., Fryer C. L., Berczik P., Hurley J. R., Spurzem R., Wang L., 2020, *A&A*, **639**, A41  
 Baron E., Cooperstein J., Kahana S., Nomoto K., 1987, *ApJ*, **320**, 304  
 Belloni D., Askar A., Giersz M., Kroupa P., Rocha-Pinto H. J., 2017, *MNRAS*, **471**, 2812  
 Bodensteiner J., et al., 2020, *A&A*, **641**, A43  
 Bovy J., 2015, *ApJS*, **216**, 29  
 Casares J., Jonker P. G., Israelian G., 2017, X-Ray Binaries. p. 1499, doi:10.1007/978-3-319-21846-5\_111  
 Chakrabarti S., et al., 2023, *AJ*, **166**, 6  
 Chawla C., Chatterjee S., Breivik K., Moorthy C. K., Andrews J. J., Sanderson R. E., 2022, *ApJ*, **931**, 107  
 Claeyns J. S. W., Pols O. R., Izzard R. G., Vink J., Verbunt F. W. M., 2014, *A&A*, **563**, A83  
 Dan M., Rosswog S., Brüggen M., Podsiadlowski P., 2014, *MNRAS*, **438**, 14  
 Dessart L., Burrows A., Ott C. D., Livne E., Yoon S. C., Langer N., 2006, *ApJ*, **644**, 1063  
 Di Carlo U. N., Agrawal P., Rodriguez C. L., Breivik K., 2023, arXiv e-prints, p. [arXiv:2306.13121](https://arxiv.org/abs/2306.13121)  
 El-Badry K., 2024, arXiv e-prints, p. [arXiv:2403.12146](https://arxiv.org/abs/2403.12146)  
 El-Badry K., Burdge K. B., 2022, *MNRAS*, **511**, 24  
 El-Badry K., Quataert E., 2020, *MNRAS*, **493**, L22  
 El-Badry K., Quataert E., 2021, *MNRAS*, **502**, 3436  
 El-Badry K., Burdge K. B., Mróz P., 2022a, *MNRAS*, **511**, 3089  
 El-Badry K., Seeburger R., Jayasinghe T., Rix H.-W., Almada S., Conroy C., Price-Whelan A. M., Burdge K., 2022b, *MNRAS*, **512**, 5620  
 El-Badry K., et al., 2023a, *The Open Journal of Astrophysics*, **6**, 28  
 El-Badry K., et al., 2023b, *MNRAS*, **518**, 1057  
 El-Badry K., et al., 2023c, *MNRAS*, **521**, 4323  
 El-Badry K., et al., 2024, arXiv e-prints, p. [arXiv:2402.06722](https://arxiv.org/abs/2402.06722)  
 Ferrand G., Tanikawa A., Warren D. C., Nagataki S., Safi-Harb S., De-courchelle A., 2022, *ApJ*, **930**, 92  
 Fryer C., Benz W., Herant M., Colgate S. A., 1999, *ApJ*, **516**, 892  
 Fryer C. L., Belczynski K., Wiktorowicz G., Dominik M., Kalogera V., Holz D. E., 2012, *ApJ*, **749**, 91  
 Gaia Collaboration et al., 2023a, *A&A*, **674**, A1  
 Gaia Collaboration et al., 2023b, *A&A*, **674**, A34  
 Geier S., Dorsch M., Dawson H., Pelisoli I., Munday J., Marsh T. R., Schaf-fenroth V., Heber U., 2023, *A&A*, **677**, A11  
 Generozov A., Perets H. B., 2023, arXiv e-prints, p. [arXiv:2312.03066](https://arxiv.org/abs/2312.03066)  
 Gessner A., Janka H.-T., 2018, *ApJ*, **865**, 61  
 Giesers B., et al., 2018, *MNRAS*, **475**, L15  
 Gronow S., Collins C., Ohlmann S. T., Pakmor R., Kromer M., Seitenzahl I. R., Sim S. A., Röpke F. K., 2020, *A&A*, **635**, A169  
 Guillotin J., Dan M., Ramirez-Ruiz E., Rosswog S., 2010, *ApJ*, **709**, L64  
 Heggie D. C., 1975, *MNRAS*, **173**, 729  
 Hirai R., Mandel I., 2022, *ApJ*, **937**, L42  
 Hobbs G., Lorimer D. R., Lyne A. G., Kramer M., 2005, *MNRAS*, **360**, 974  
 Howil K., et al., 2024, Uncovering the Invisible: A Study of Gaia18ajz, a Candidate Black Hole Revealed by Microlensing ([arXiv:2403.09006](https://arxiv.org/abs/2403.09006))  
 Hurley J. R., Pols O. R., Tout C. A., 2000, *MNRAS*, **315**, 543  
 Hurley J. R., Tout C. A., Pols O. R., 2002, *MNRAS*, **329**, 897  
 Ivanova N., Heinke C. O., Rasio F. A., Belczynski K., Fregeau J. M., 2008, *MNRAS*, **386**, 553  
 Iwasawa M., Tanikawa A., Hosono N., Nitadori K., Muranushi T., Makino J., 2016, *PASJ*, **68**, 54  
 Iwasawa M., Oshino S., Fujii M. S., Hori Y., 2017, *PASJ*, **69**, 81  
 Iwasawa M., Namekata D., Nitadori K., Nomura K., Wang L., Tsubouchi M., Makino J., 2020, *PASJ*, **72**, 13  
 Jayasinghe T., et al., 2021, *MNRAS*, **504**, 2577  
 Jayasinghe T., et al., 2022, *MNRAS*, **516**, 5945  
 Jayasinghe T., Rowan D. M., Thompson T. A., Kochanek C. S., Stanek K. Z., 2023, *MNRAS*, **521**, 5927  
 Jones S., et al., 2013, *ApJ*, **772**, 150  
 Kashyap R., Fisher R., García-Berro E., Aznar-Siguán G., Ji S., Lorén-Aguilar P., 2015, *ApJ*, **800**, L7  
 Kashyap R., Haque T., Lorén-Aguilar P., García-Berro E., Fisher R., 2018, *ApJ*, **869**, 140  
 Kotko I., Banerjee S., Belczynski K., 2024, arXiv e-prints, p. [arXiv:2403.13579](https://arxiv.org/abs/2403.13579)  
 Kremer K., Fuller J., Piro A. L., Ransom S. M., 2023, *MNRAS*, **525**, L22  
 Kroupa P., 1995a, *MNRAS*, **277**, 1491  
 Kroupa P., 1995b, *MNRAS*, **277**, 1507  
 Kroupa P., 2001, *MNRAS*, **322**, 231  
 Küpper A. H. W., Maschberger T., Kroupa P., Baumgardt H., 2011, *MNRAS*, **417**, 2300  
 Lam C. Y., et al., 2022, *ApJ*, **933**, L23  
 Lennon D. J., Dufton P. L., Villaseñor J. I., Evans C. J., Langer N., Saxton R., Monageng I. M., Toonen S., 2022, *A&A*, **665**, A180  
 Liu J., et al., 2019, *Nature*, **575**, 618  
 Longo Micchi L. F., Radice D., Chirenti C., 2023, *MNRAS*, **525**, 6359  
 Miyaji S., Nomoto K., Yokoi K., Sugimoto D., 1980, *PASJ*, **32**, 303  
 Moe M., Di Stefano R., 2017, *ApJS*, **230**, 15  
 Mori M., Sawada R., Suwa Y., Tanikawa A., Kashiyama K., Murase K., 2023, arXiv e-prints, p. [arXiv:2306.17381](https://arxiv.org/abs/2306.17381)  
 Nomoto K., 1982, *ApJ*, **257**, 780  
 Nomoto K., 1984, *ApJ*, **277**, 791  
 Nomoto K., 1987, *ApJ*, **322**, 206  
 Nomoto K., Kondo Y., 1991, *ApJ*, **367**, L19

Oshino S., Funato Y., Makino J., 2011, *PASJ*, **63**, 881

Pakmor R., Kromer M., Röpke F. K., Sim S. A., Ruiter A. J., Hillebrandt W., 2010, *Nature*, **463**, 61

Pakmor R., Hachinger S., Röpke F. K., Hillebrandt W., 2011, *A&A*, **528**, A117

Pakmor R., Edelmann P., Röpke F. K., Hillebrandt W., 2012a, *MNRAS*, **424**, 2222

Pakmor R., Kromer M., Taubenberger S., Sim S. A., Röpke F. K., Hillebrandt W., 2012b, *ApJ*, **747**, L10

Pakmor R., Kromer M., Taubenberger S., Springel V., 2013, *ApJ*, **770**, L8

Pakmor R., Zenati Y., Perets H. B., Toonen S., 2021, *MNRAS*, **503**, 4734

Perets H. B., et al., 2010, *Nature*, **465**, 322

Philipov A., Kramer M., 2022, *ARA&A*, **60**, 495

Podsiadlowski P., Langer N., Poelarends A. J. T., Rappaport S., Heger A., Pfahl E., 2004, *ApJ*, **612**, 1044

Portegies Zwart S. F., McMillan S. L. W., Gieles M., 2010, *ARA&A*, **48**, 431

Rastello S., Iorio G., Mapelli M., Arca-Sedda M., Di Carlo U. N., Escobar G. J., Shenar T., Torniamenti S., 2023, *MNRAS*, **526**, 740

Rivinius T., Baade D., Hadrava P., Heida M., Klement R., 2020, *A&A*, **637**, L3

Rowan D. M., Thompson T. A., Jayasinghe T., Kochanek C. S., Stanek K. Z., 2024, *arXiv e-prints*, p. arXiv:2401.09531

Ruiter A. J., 2019, *Proceedings of the International Astronomical Union*, **15**, 1–15

Sahu K. C., et al., 2022, *ApJ*, **933**, 83

Sana H., et al., 2012, *Science*, **337**, 444

Saracino S., et al., 2022, *MNRAS*, **511**, 2914

Sato Y., Nakasato N., Tanikawa A., Nomoto K., Maeda K., Hachisu I., 2015, *ApJ*, **807**, 105

Sato Y., Nakasato N., Tanikawa A., Nomoto K., Maeda K., Hachisu I., 2016, *ApJ*, **821**, 67

Schwab J., Quataert E., Bildsten L., 2015, *MNRAS*, **453**, 1910

Shahaf S., Hallakoun N., Mazeh T., Ben-Ami S., Rekhi P., El-Badry K., Toonen S., 2023a, *arXiv e-prints*, p. arXiv:2309.15143

Shahaf S., Bashi D., Mazeh T., Faigler S., Arenou F., El-Badry K., Rix H. W., 2023b, *MNRAS*, **518**, 2991

Shen K. J., et al., 2018, *ApJ*, **865**, 15

Shenar T., et al., 2022, *Nature Astronomy*, **6**, 1085

Shikauchi M., Tsuna D., Tanikawa A., Kawanaka N., 2023, *ApJ*, **953**, 52

Tanikawa A., Nomoto K., Nakasato N., 2018, *ApJ*, **868**, 90

Tanikawa A., Nomoto K., Nakasato N., Maeda K., 2019, *ApJ*, **885**, 103

Tanikawa A., Hattori K., Kawanaka N., Kinugawa T., Shikauchi M., Tsuna D., 2023, *ApJ*, **946**, 79

Tanikawa A., Cary S., Shikauchi M., Wang L., Fujii M. S., 2024, *MNRAS*, **527**, 4031

Thompson T. A., et al., 2019, *Science*, **366**, 637

Toonen S., Nelemans G., Portegies Zwart S., 2012, *A&A*, **546**, A70

Wang L., Nitadori K., Makino J., 2020a, *MNRAS*, **493**, 3398

Wang L., Iwasawa M., Nitadori K., Makino J., 2020b, *MNRAS*, **497**, 536

Webbink R. F., 1984, *ApJ*, **277**, 355

Woosley S. E., Baron E., 1992, *ApJ*, **391**, 228

Woosley S. E., Taam R. E., Weaver T. A., 1986, *ApJ*, **301**, 601

Yamaguchi N., et al., 2024, *MNRAS*, **527**, 11719

Zenati Y., Perets H. B., Dessart L., Jacobson-Galán W. V., Toonen S., Rest A., 2023, *ApJ*, **944**, 22

Zheng L.-L., et al., 2023, *Science China Physics, Mechanics, and Astronomy*, **66**, 129512

van den Heuvel E. P. J., 2007, in di Salvo T., Israel G. L., Piersant L., Burderi L., Matt G., Tornambe A., Menna M. T., eds, American Institute of Physics Conference Series Vol. 924, The Multicolored Landscape of Compact Objects and Their Explosive Origins. pp 598–606 (arXiv:0704.1215), doi:10.1063/1.2774916

van den Heuvel E. P. J., Tauris T. M., 2020, *Science*, **368**, eaba3282